Journal of Computational Physics 294 (2015) 605–618

Contents lists available at ScienceDirect

Journal of Computational Physics

www.elsevier.com/locate/jcp

On the search of more stable second-order lattice-Boltzmann schemes in confined flows

D.R. Golbert [a,b], P.J. Blanco [a,b,*], A. Clausse [c], R.A. Feijóo [a,b]

[a] Laboratório Nacional de Computação Científica, Getúlio Vargas 333, Quitandinha, 25651-075 Petrópolis, RJ, Brazil
[b] Instituto Nacional de Ciência e Tecnologia em Medicina Assistida por Computação Científica, Petrópolis, RJ, Brazil
[c] CNEA–CONICET and Universidad Nacional del Centro, 7000 Tandil, Argentina

ARTICLE INFO

Article history:
Received 7 February 2014
Received in revised form 9 March 2015
Accepted 21 March 2015
Available online 8 April 2015

Keywords:
Linear stability
Incompressible flow
von Neumann analysis

ABSTRACT

The von Neumann linear analysis, restricted by a heuristic selection of wave-number vectors was applied to the search of explicit lattice Boltzmann schemes which exhibit more stability than existing methods. The relative stability of the family members of quasi-incompressible collision kernels, for the Navier–Stokes equations in confined flows, was analyzed. The linear stability analysis was simplified by assuming a uniform velocity level over the whole domain, where only the wave numbers of the first harmonic normal to the flow direction were permitted. A singular equilibrium function that maximizes the critical velocity level was identified, which was afterwards tested in particular cases of confined flows of interest, validating the resulting procedure.

1. Introduction

Since its introduction in the 1980s the lattice Boltzmann method (LBM) has overcome several refinements and extensions, and has become a promising numerical scheme for simulating complex fluid dynamics in the most varied applications. For instance, LBM was successfully applied to the modeling of homogeneous turbulence and multi-phase flows in porous media [1–3], blood flow in macro vessels [4–8] and micro vessels [9–11].

Differing from the conventional methods, based on a direct discretization of continuum macroscopic Navier–Stokes equations, LBM is a mesoscopic particle-based method derived from the Lattice-Gas Cellular Automata [12] and the Boltzmann Equation [13]. Its basic idea consists in building a simplified kinetic model in such a way that the average properties of the system are governed by a certain set of field equations.

A key point for the stability of this method is the collision process of the particles, associated to an equilibrium distribution that is constructed with the macroscopic variables. Most approaches use the BGK scheme for the collision process. Based on this model, previous works have studied the stability of the model. Sterling and Chen [14] report some stability results for a subset of the parameter space for BGK in hexagonal, square and cubic lattices, finding a critical velocity that increases monotonically with the relaxation parameter until a saturation value is reached. Worthing et al. [15] extended the linear analysis to address the destabilizing role of background shear, finding the stability criterion $N < \mathrm{Re}^{0.56}$, where N is the number of mesh points in the shearing direction and Re is the Reynolds number. Tosi et al. [16] studied the non-linear stability properties of entropic schemes comparing them with positivity-enforcing schemes in a two-dimensional cavity

* Corresponding author at: Laboratório Nacional de Computação Científica, Getúlio Vargas 333, Quitandinha, 25651-075 Petrópolis, RJ, Brazil.
E-mail address: pjblanco@lncc.br (P.J. Blanco).

http://dx.doi.org/10.1016/j.jcp.2015.03.065
0021-9991/

flow, showing that both methods achieve substantial stability enhancements over the standard single-time relaxation LBM. Brownlee et al. [17] studied the interplay between stability and accuracy in LBM, identified the main instability mechanisms and proposed simple recipes for stabilization, such as the addition of local artificial dissipation to control the positivity and local blowup. Servan-Camas and Tsai [18] analyzed the stability of the BGK scheme and found that non-negativity of the equilibrium distribution function is a sufficient condition for linear stability and a necessary condition when the relaxation time is very close to 0.5. Rheinländer [19] discussed the stability structure of LBM from the perspective of matrix analysis and applied the results to different collision operators. Ricot et al. [20] proposed the use of spatial filters in order to stabilize LBM. El-Amin et al. [21] studied the stability of a finite-difference based LBM-BGK scheme, finding ranges of the parameter space that have stable solutions.

More recently, the stability of the second and third order schemes were compared showing that as expected the latter presents increased stability ranges [22–24]. Derivations of third-order LBM schemes using different procedures where proposed by Shan et al. [25], Philippi et al. [26], Siebert et al. [27], Shan [28] and Mattila et al. [29]. In any case, even to the present most engineering applications apply the second-order BGK scheme for the collision process [30–38]. As Montessori et al. [23] recently pointed out: "Indeed, the LBGK has known a very rapid surge of popularity and still holds the lead among the various LB variants available today, notwithstanding a number of limitations. Among others, the loss of numerical stability at low viscosity (high-Reynolds) appears particularly constraining for a number of engineering applications... LBGK is also (over) criticized for being inaccurate, even though such an inaccuracy often amounts to a few percents. While unacceptable for accurate and systematic convergence studies, this is certainly viable for most applications exposed to many additional sources of physical and numerical inaccuracy. Hence, in many instances, there are definitely no apologies to be offered for using LBGK and variants thereof". Nevertheless, it should be stressed that increasing the order of the equilibrium distribution model towards improved lattice Boltzmann equations benefits both stability and accuracy.

A number of variations of the second-order BGK scheme with improved performance were also proposed [39–41]. Also several regularization procedures of the equilibrium distributions have been proposed to increase the stability range of LBM schemes. Latt and Chopard [42] proposed regularized distribution functions that suppress non-equilibrium modes, which increased the stability in numerical tests of 2D lid-driven cavity flows. Montessori et al. [23] corroborated these findings and showed that the stabilizing effects extend to 3D cavity flows. Zhang et al. [43] showed other regularizations achieved by means of Hermite polynomials. Chen et al. [44] proposed a regularization by aleatory rotations of the discrete velocity set, although in this case some procedure for associating the solutions in rotated grids is needed.

In the present article, the results of a thorough exploration of the stability of a general class of quasi-incompressible LBM schemes are presented. Differing from other approaches, these LBM schemes maintain the single relaxation approach with small changes in the equilibrium distribution. Furthermore, an analytical guiding criterion is derived from a restricted linear stability analysis (taking into account the confinement of the flows), which afterwards is tested in three numerical simulations of confined flows to verify the stability improvements for a wide range of numerical parameters.

2. Incompressible lattice Boltzmann schemes

From the numerical perspective, LBM can be seen as an explicit method to solve transport equations using more variables than those strictly necessary to characterize the macroscopic phenomena. It is based on the movement and collision of particles described by the lattice Boltzmann equation:

$$f_i(\vec{x}+\vec{e}_i\Delta x, t+\Delta t) = f_i(\vec{x},t) - \frac{1}{\tau}\left[f_i(\vec{x},t) - f_i^e(\vec{x},t)\right], \quad \text{for } i=0,\ldots,\ell, \tag{1}$$

where $f_i(\vec{x},t)$ represents the particles distribution density at position $\vec{x}$ and time t, undergoing a displacement $\vec{e}_i\Delta x$ in a time step Δt, τ is the relaxation parameter and ℓ is the number of non-null lattice directions.

Vectors $\vec{e}_i$ form a finite set of directions that restrict the movement of the particles among the points of space where the solution is computed. In what follows the so called D2Q9 model will be used, which is given by the set:

$$\begin{aligned} &\vec{e}_0=(0,0); \quad \vec{e}_1=(1,0); \quad \vec{e}_2=(0,1); \quad \vec{e}_3=(-1,0); \quad \vec{e}_4=(0,-1);\\ &\vec{e}_5=(1,1); \quad \vec{e}_6=(-1,1); \quad \vec{e}_7=(-1,-1); \quad \vec{e}_8=(1,-1). \end{aligned} \tag{2}$$

For simplicity, from now on, we will assume that the index i varies from 0 to 8.

Using an asymptotic expansion, it has been demonstrated that the lattice Boltzmann equation (1) approximates the Navier–Stokes equations, provided that the so called equilibrium function $f_i^e(\vec{x},t)$ satisfies a set of constitutive conditions related to the moments of $f_i(\vec{x},t)$ with respect to $\vec{e}_i$. Comprehensive reviews of this procedure can be found elsewhere [2,45,46]. A popular scheme complying with these conditions is the classical BGK:

$$f_i^e(\vec{x},t) = w_\sigma\rho\left[1+3\frac{(v\vec{e}_i\cdot\vec{u})}{v^2} - \frac{3}{2}\frac{u^2}{v^2} + \frac{9}{2}\frac{(v\vec{e}_i\cdot\vec{u})^2}{v^4}\right], \tag{3}$$

where $v=\Delta x/\Delta t$ is the particle speed and $u^2=\vec{u}\cdot\vec{u}$. The macroscopic quantities:

$$\rho = \sum_i f_i(\vec{x},t) \quad \text{and} \quad \vec{u} = \frac{1}{\rho}\sum_i v\vec{e}_i f_i(\vec{x},t) \tag{4}$$

are the particle-number density and average velocity. The index σ is 0 for the resting particles, and 1 and 2 for the particles moving in the Cartesian and diagonal directions, respectively. The corresponding weight coefficients are $w_0 = 4/9$, $w_1 = 1/9$ and $w_2 = 1/36$. In such case, the relaxation parameter τ is related to the kinematic viscosity of the fluid by [45]:

$$\upsilon = (2\tau - 1)\Delta x^2/(6\Delta t) \tag{5}$$

and the pressure is calculated using the isothermal equation of state:

$$p = \rho\frac{v^2}{3}. \tag{6}$$

There are many other possible relations between $f_i^e(\vec{x}, t)$ and $f_i(\vec{x}, t)$ that lead to the same differential limit. One of the main differences between all these alternatives is the numerical stability of the resulting scheme, which is a crucial characteristic in LBM, being an explicit, and therefore conditionally stable, method. For instance, for the stability problems encountered in LBM implementations when dealing with special applications in hemodynamics see Golbert et al. [8]. A particularly interesting and useful scheme was proposed by He and Luo [45], as a more stable extension of BGK, which approximates the quasi-incompressible Navier–Stokes equations, namely:

$$f_i^e = w_\sigma\left\{\rho + \rho_0\left[3\frac{(v\vec{e}_i\cdot\vec{u})}{v^2} - \frac{3}{2}\frac{u^2}{v^2} + \frac{9}{2}\frac{(v\vec{e}_i\cdot\vec{u})^2}{v^4}\right]\right\}, \tag{7}$$

where ρ_0 is the constant density level. The macroscopic quantities are recovered as in Eq. (4), but ρ is replaced by ρ_0 when recovering the velocity ($\vec{u}$).

Taking the form of Eq. (7) as a reference, one can define a family of equilibrium functions, given by:

$$f_i^e = A_\sigma\rho + \rho_0\left[B_\sigma\frac{(v\vec{e}_i\cdot\vec{u})}{v^2} + C_\sigma\frac{u^2}{v^2} + D_\sigma\frac{(v\vec{e}_i\cdot\vec{u})^2}{v^2}\right], \tag{8}$$

where A_σ, B_σ, C_σ and D_σ is the family of parameters.

In order to approximate the incompressible Navier–Stokes equation, f_i^e should satisfy [45]:

$$\sum_i f_i^e = \rho, \tag{9}$$

$$\sum_i f_i^e e_{i,\alpha} v = \rho_0 u_\alpha, \tag{10}$$

$$\sum_i f_i^e e_{i,\alpha} e_{i,\beta} v^2 = \frac{v^2}{3}\rho\delta_{\alpha\beta} + \rho_0 u_\alpha u_\beta, \tag{11}$$

$$\sum_i f_i^e e_{i,\alpha} e_{i,\beta} e_{i,\gamma} v^3 = \frac{v^2}{3}\rho_0(\delta_{\alpha\beta}u_\gamma + \delta_{\gamma\alpha}u_\beta + \delta_{\beta\gamma}u_\alpha), \tag{12}$$

where the term $e_{i,\alpha}$ is the projection of $\vec{e}_i$ on the α-axis ($\alpha = x$ or y).

By applying the equilibrium distribution of Eq. (8) to Eqs. (9)–(12) only two free parameters are left, which are chosen to be A_2 and C_2. The other parameters are given by the following relations:

$$A_1 = \frac{1}{6} + 2A_2, \tag{13}$$

$$A_0 = 1 - 4(A_1 + A_2), \tag{14}$$

$$B_1 = \frac{1}{2} - 2B_2, \tag{15}$$

$$C_1 = -2(D_2 + C_2), \tag{16}$$

$$C_0 = -4(C_1 + C_2 + D_2) - 2D_1. \tag{17}$$

The remaining parameters are $B_2 = 1/12$, $D_1 = 1/2$ and $D_2 = 1/8$. He and Luo [46] scheme corresponds to $A_2 = 1/36$ and $C_2 = -1/24$, while Yeomans [46] proposed the scheme $A_2 = 1/24$ and $C_2 = -1/16$.

In this work, the velocity boundary conditions are imposed using the method proposed by Guo et al. [47], and the pressure boundary conditions with the method proposed by Zou and He [48].

The rest of the paper is dedicated to perform an exploratory search of a pair of parameters A_2 and C_2 that leads to an LBM scheme which is more stable than schemes published in previous works. A remarkable point here is that modifications of the parameters A_2 and C_2 are very simple to be implemented and can have great influence in the numerical stability.

3. Stability analysis

Let us consider a case of a flow for which there exists a steady state $\tilde{f}_i(\vec{x})$ satisfying:

$$\tilde{f}_i(\vec{x}+\vec{e}_i\Delta x) = \tilde{f}_i(\vec{x}) - \frac{1}{\tau}\left[\tilde{f}_i(\vec{x}) - \tilde{f}_i^e(\vec{x})\right]. \tag{18}$$

To study the stability of the steady-state, the distribution function is written as the sum of the steady-state $\tilde{f}_i(\vec{x})$ and a time-dependent perturbation, that is:

$$f_i(\vec{x},t) = \tilde{f}_i(\vec{x}) + \delta f_i(\vec{x},t). \tag{19}$$

Replacing Eq. (19) in Eq. (18) and linearizing the equilibrium distribution $f_i^e(\vec{x},t)$ around the steady-state gives:

$$\delta f_i(\vec{x}+\vec{e}_i\Delta x, t+\Delta t) = \delta f_i(\vec{x},t) - \frac{1}{\tau}\left[\delta f_i(\vec{x},t) - \sum_j J_{ij}(\vec{x})\delta f_j(\vec{x},t)\right], \tag{20}$$

where

$$J_{ij}(\vec{x}) = \frac{\partial f_i^e}{\partial f_j}. \tag{21}$$

Using the following results:

$$\frac{\partial \rho}{\partial f_j} = 1, \tag{22}$$

$$\frac{\partial}{\partial f_j}(v\vec{e}_i\cdot\vec{u}) = v\vec{e}_i\cdot\frac{\partial\vec{u}}{\partial f_j} = \frac{v\vec{e}_i\cdot v\vec{e}_j}{\rho_0}, \tag{23}$$

$$\frac{\partial}{\partial f_j}(\vec{u}\cdot\vec{u}) = 2\vec{u}\cdot\frac{\partial\vec{u}}{\partial f_j} = 2\frac{(\vec{u}\cdot v\vec{e}_j)}{\rho_0}, \tag{24}$$

$$\frac{\partial}{\partial f_j}(v\vec{e}_i\cdot\vec{u})^2 = \frac{2}{\rho_0}(v\vec{e}_i\cdot v\vec{e}_j)(v\vec{e}_i\cdot\vec{u}), \tag{25}$$

the Jacobian can be written as:

$$J_{ij} = A_\sigma + B_\sigma\frac{(v\vec{e}_i\cdot v\vec{e}_j)}{v^2} + 2C_\sigma\frac{(v\vec{e}_j\cdot\vec{u})}{v^2} + 2D_\sigma\frac{(v\vec{e}_i\cdot v\vec{e}_j)(v\vec{e}_i\cdot\vec{u})}{v^4}. \tag{26}$$

Following the von Neumann analysis performed by Sterling and Chen [14], let us evaluate the Jacobian J_{ij} at a fixed constant value U of the steady-state velocity, and write the perturbation $\delta f_i(\vec{x},t)$ as:

$$\delta f_i(\vec{x},t) = e^{-\frac{2\pi\iota}{\Delta x}(\vec{k}\cdot\vec{x})}F_i(t), \tag{27}$$

where $\iota = \sqrt{-1}$.

Combining Eqs. (20) and (27) gives:

$$F_i(t+\Delta t) = \sum_j \Gamma_{ij}F_j(t), \tag{28}$$

where

$$\Gamma_{ij} = e^{2\pi\iota(\vec{k}\cdot\vec{e}_i)}\left[\left(1-\tau^{-1}\right)\delta_{ij} + \tau^{-1}J_{ij}\right]. \tag{29}$$

Eq. (28) is a set of 9 linear difference equations whose general solution can be written as a linear combination of terms proportional to q_i^n, where n is the number of time steps and q_i are the eigenvalues of Γ_{ij}, which in general are complex. The linear stability condition is ensured by:

$$r = \max_i |q_i| \le 1. \tag{30}$$

The spectral radius r depends on the wave number vector $\vec{k}$, the velocity level U, the relaxation parameter τ, and the parameters of the equilibrium distribution A_σ, B_σ, C_σ and D_σ. The goal of the present analysis is to find the combination of such parameters that improves the stability of the scheme by increasing the critical velocity level (U_{crit}) for which r approaches unity.

It should be noted that this is a very special case, for J_{ij} in general depends on $\vec{x}$ and $\delta f_i(\vec{x},t)$ is actually a combination of many terms with different $\vec{k}$. However, the study of Eq. (28) can be considered as a sufficient condition for linear stability, and we propose here to use it in order to guide the assessment of the relative degree of stability of different LBM schemes [14,15]. Based on the results of this assessment, subsequent numerical tests of particular cases will be performed to confirm the spectral results.

Table 1
Parameters of the four analyzed equilibrium distributions (see Eq. (8)). For the BGK scheme, replace ρ_0 for ρ in Eq. (8).

LBM scheme	A_0	A_1	A_2	B_1	B_2	C_0	C_1	C_2	D_1	D_2
BGK	0	2/9	1/36	1/3	1/12	−2/3	−1/6	−1/24	1/2	1/8
He and Luo [45]	0	2/9	1/36	1/3	1/12	−2/3	−1/6	−1/24	1/2	1/8
Yeomans [46]	−1/6	1/4	1/24	1/3	1/12	−3/4	−1/8	−1/16	1/2	1/8
Present scheme	0.0798	0.2089	0.0211	1/3	1/12	−0.5719	−0.214	−0.018	1/2	1/8

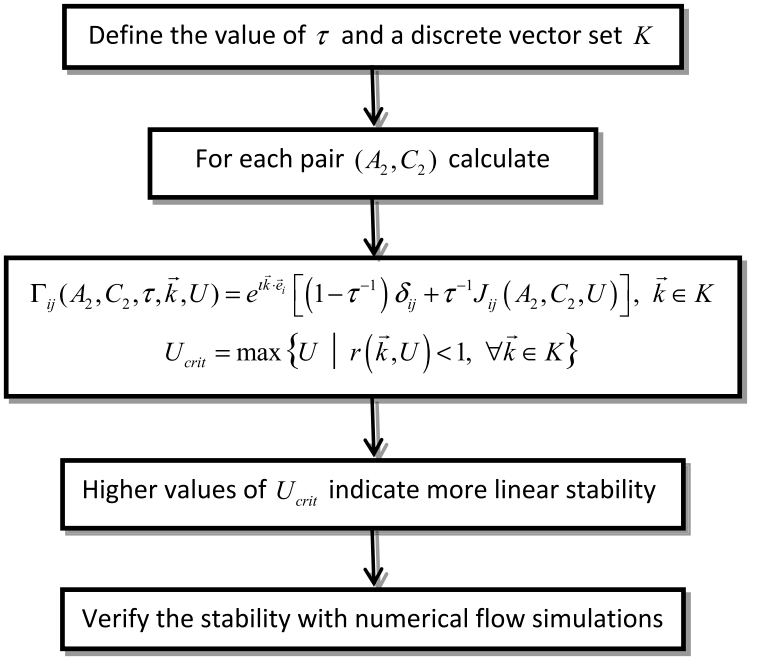

Fig. 1. Diagram of the heuristic search of more stable LBM schemes, guided by the spectral radius r and a selection of perturbations.

4. Results

This section starts with a description of the methodology performed to find more stable schemes for a general class of quasi-incompressible lattice Boltzmann equations, Eq. (8). Here a new scheme is presented, as an optimized choice of the parameters A_σ, B_σ, C_σ and D_σ for a certain class of confined flows.

In the sequence, the numerical stability of the new scheme is compared with other schemes in cases of interest where the numerical solutions or known analytical solutions can be used to assess the error. More specifically, we compare the results obtained in plane Poiseuille and Couette flows and in a Driven Cavity (all in equal geometries of aspect ratio 2×1), varying the relaxation parameter τ ($\tau = 0.5 + 0.5/n,\ n = 1, \ldots, 12$), the number of points in the transversal direction ($L_y/\Delta x = 10, 15, 20, 30, 40, 60$) and the Reynolds number, by the four LBM schemes detailed in Table 1.

Over 100 000 simulations were performed on a Bull Cluster at the National Laboratory for Scientific Computation (LNCC, Brazil), consisting of 100 blades with 36 GB of RAM and 2 Intel Xeon X5550 processors of 2.67 GHz each.

4.1. Stability maps

The standard incompressible BGK model proposed by He and Luo [45] was taken as reference from which alternative schemes are explored in what follows.

The searching procedure of more stable LBM schemes, with an equilibrium distribution as in Eq. (8), is depicted in Fig. 1. For a given τ and a set of perturbations K, the spectral radius of the matrix Γ_{ij} can be calculated as a function of the velocity level U, for each set of parameters of the equilibrium function (A_σ, B_σ, C_σ and D_σ, which are determined by A_2 and C_2 as shown in Eqs. (13)–(17). The stability margin is then determined by the condition $r(\vec{k}, U) = 1$. With this information, particular equilibrium distributions can be selected and their stability influence verified with numerical simulations. The eigenvalues of Γ_{ij} were calculated numerically using the FORTRAN subroutine DEVCCG of the IMSL Library in double precision.

Since the wave number is a vector, in principle the whole range of values of k_x and k_y would need to be swept in the interval $(-1, 1)$. For example, assuming the He and Luo [45] scheme, $\tau = 0.5001$ and setting $\vec{k}$ parallel to the flow

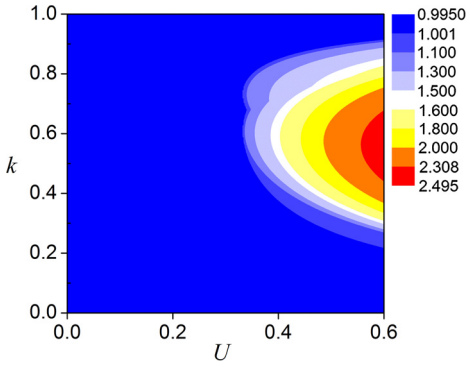

Fig. 2. Map of the spectral radius (r) of He and Luo [45] scheme when the wave number vector is parallel to the steady-state flow ($\tau = 0.5001$). (For interpretation of the colors in this figure, the reader is referred to the web version of this article.)

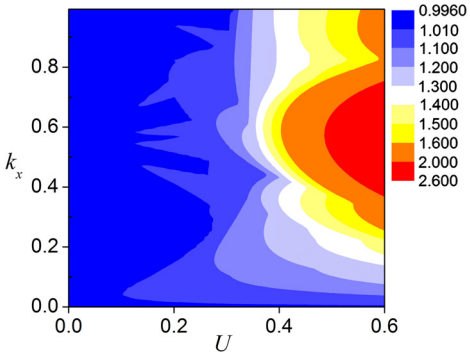

Fig. 3. Map of the spectral radius (r) of He and Luo [45] scheme when all the wave number components normal to the flow, k_y, are tested ($\tau = 0.5001$). (For interpretation of the colors in this figure, the reader is referred to the web version of this article.)

results in the r-map shown in Fig. 2. The most dangerous wavenumber is $k = 0.73$ (modulus of $\vec{k}$), which corresponds to a critical velocity $U_{crit} = 0.33$ (in units of $\Delta x/\Delta t$). However, in principle there can be a more unstable wave-number vector $\vec{k}$ not parallel to the velocity. Testing for the whole range of allowed transversal wave numbers (k_y), for each pair (k_x, U), leads to the map showed in Fig. 3. The critical velocity decreases in this case to 0.1. The form of the contour lines as they approach the stability boundary, $r = 1$, shows that different values of k_y contribute triggering different instability modes, producing "fingers" that decrease the critical velocity. Other authors [15,20] studied approximate solutions to the complete eigenvalue problem, which involves the spatial dependence of the matrix Γ_{ij}, finding that the boundary conditions in the transversal direction influence the stability. For the purpose of an explorative analysis, aimed at identifying more stable LBM schemes in particular cases of interest, it can be assumed that there is a fixed confinement in the transversal direction. This confinement is always present in internal flows and restricts the values of k_y to a discrete set consistent with standing waves confined in a finite length L_y, that is [15,20]:

$$k_y = \frac{1}{n}; \quad 1 \leq |n| \leq \frac{L_y}{\Delta x}. \tag{31}$$

Since usually the lowest mode is the dominant, in order to simplify the heuristics we propose to analyze relative variations of the stability margin assuming $k_y = \Delta x/L_y$ ($n = L_y/\Delta x$). The resulting critical velocity would hopefully provide a guide to the search of more stable LBM schemes on this particular domain of geometries (see Fig. 1).

Fig. 4 shows the stability thresholds of the schemes suggested by He and Luo [45] and Yeomans [46], for $\tau = 0.501$ and confinement ratio $L_y/\Delta x = 10$. It can be seen that the Yeomans [46] scheme is unconditionally unstable. In order to identify a more stable scheme, a comprehensive search was performed over a large range of parameters A_2 and C_2 (see Eq. (8)). Fig. 5 shows the critical velocity level calculated for each pair (A_2, C_2) setting $L_y/\Delta x = 10$ and $\tau = 0.501$. The maximum critical velocity U_{crit} (i.e., the most stable pair) corresponds neither to the scheme proposed by He and Luo [45] nor by Yeomans [46]. Similar maps are found for other ratios $L_y/\Delta x$. Fig. 6 shows the combined map of U_{crit}, with $L_y/\Delta x$ ranging between 10 and 60. The maximum critical velocity, $U_{crit} = 0.25$, corresponds to the pair $A_2 = 0.0211242$ and $C_2 = -0.0179776$. The stability threshold of this scheme is compared in Fig. 4 with the previous schemes, which confirms that the proposed scheme is in effect more stable.

The optimum set of parameters is given in Table 1. It is interesting to observe in Fig. 7 the spectral-radius map of the proposed scheme resulting from the complete sweep of possible values of the transversal wave number k_y. Surprisingly, if any value of k_y is allowed, this scheme is unstable for all velocity levels. An unstable mode around $k_x \sim 0.55$ is possible,

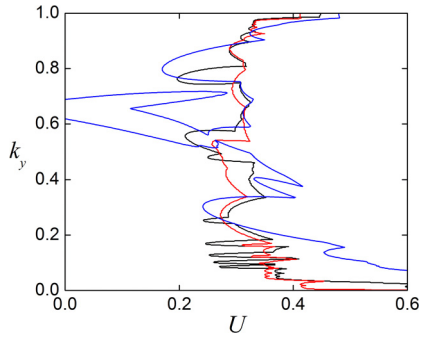

Fig. 4. Stability margins for $\tau = 0.501$, $k_y = 2\pi/L_y$, $L_y/\Delta x = 10$. He and Luo [45] (black), Yeomans [46] (blue), proposed scheme (red). (For interpretation of the references to color in this figure legend, the reader is referred to the web version of this article.)

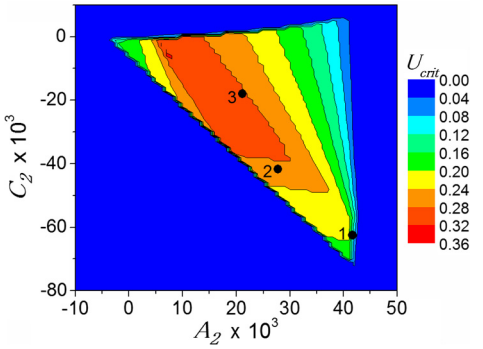

Fig. 5. Map of critical velocities (in units of $\Delta x/\Delta t$) in the space of two-parameters incompressible LBM schemes ($\tau = 0.501$, $k_y = 2\pi/L_y$, $L_y/\Delta x = 10$). Points 1, 2 and 3 correspond to Yeomans [46], He and Luo [45] and the present schemes, respectively. (For interpretation of the colors in this figure, the reader is referred to the web version of this article.)

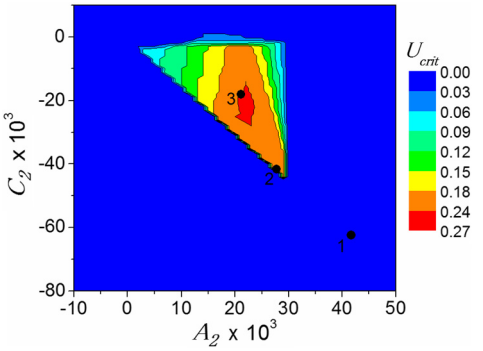

Fig. 6. Map of critical velocities (in units of $\Delta x/\Delta t$) in the space of two-parameters incompressible LB schemes ($\tau = 0.501$, $k_y = 2\pi/L_y$, $L_y/\Delta x$ ranging from 10 to 60). Points 1, 2 and 3 correspond to Yeomans [46], He and Luo [45] and the present schemes, respectively. (For interpretation of the colors in this figure, the reader is referred to the web version of this article.)

which seems to be damped by the confinement in the transversal direction when the confinement ratio $L_y/\Delta x$ is lower than 60, as we will verify in the numerical experiments that follow.

The stability of the optimum scheme ($A_2 = 0.0211$ and $C_2 = -0.018$) is compared with the stability of the standard incompressible BGK-D2Q9 scheme and with the third order D2Q9 scheme proposed by Siebert et al. [22]. Fig. 8 displays this stability analysis. While the third order scheme from [22] allows higher Reynolds numbers for most values of τ, remarkably, the model derived in the present study features better stability for τ very close to 0.5 (i.e., very low viscosities).

4.2. Poiseuille flow between parallel plates

Numerical simulations for the Poiseuille flow in a channel between parallel plates, with aspect ratio 2×1, driven by a fixed pressure gradient were carried out using the LBM schemes listed in Table 1. In all cases no-slip conditions were applied at the walls (top and bottom) and constant pressure values at the inlet (p_{in}) and the outlet (p_{out}). The density at

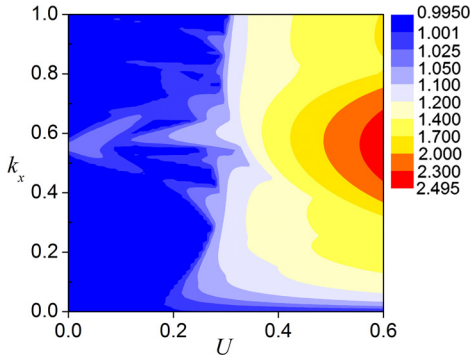

Fig. 7. Map of spectral radius of the present scheme testing all transversal wavenumbers k_y ($\tau = 0.501$). (For interpretation of the colors in this figure, the reader is referred to the web version of this article.)

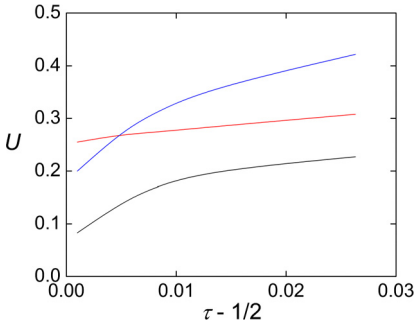

Fig. 8. Dependence of the critical fluid velocity with the viscosity parameter τ. Black: BGK, blue: third order scheme [22], red: D2Q9 scheme with optimized coefficients ($A_2 = 0.0211$ and $C_2 = -0.018$). (For interpretation of the references to color in this figure legend, the reader is referred to the web version of this article.)

the channel outlet is constant and taken as the system density level ($p_{out} = p_0 = \rho_0 v^2/3$). The calculation initiates with a channel inlet pressure (p_{in}) slightly higher than the exit (p_{out}), that is:

$$p_{in} = p_{out} + \Delta p = \frac{\rho_0 v^2}{3} + \Delta p. \tag{32}$$

The pressure drop (Δp) is chosen so that the theoretical Reynolds number *Re* (calculated with the maximum velocity) is 5, that is, from the analytical solution of the Poiseuille flow:

$$\Delta p = u_{max} 8 \nu \rho L = \frac{\nu \,\mathrm{Re}}{D} 8 \nu \rho L = \frac{40 \nu^2 \rho L}{D}, \tag{33}$$

where D is the distance between the parallel plates.

The simulation stops when the following criterion for assessing steady state is reached (for some time instant t_n):

$$\frac{\sqrt{\sum_{j=1}^{N_P} \|\vec{u}(\vec{x}_j, t_n) - \vec{u}(\vec{x}_j, t_{n-1})\|^2}}{N_P u_{max}} < 10^{-10}, \tag{34}$$

where N_P is the total number of discretization points and $\|\cdot\|$ is the Euclidean norm.

If this criterion is reached in less than $N_T = 80\,(N_P - 1)^2\,/\,(\tau - 0.5)$ time steps, then the inlet pressure is increased a quantity Δp, u_{max} is updated accordingly and the calculation continues until the steady-state criterion is reached again, and so on. If at certain point in the process the steady-state criterion is not reached after N_T time steps, or there is an overflow in the calculation, the simulation stops and the flow is considered unstable. The critical Reynolds is then defined as the maximum velocity for which the convergence criterion given by Eq. (34) was achieved.

The procedure described above was performed varying the relaxation parameter τ ($\tau = 0.5 + 0.5/n$, $n = 1, \ldots, 12$) and the number of points in the transversal direction ($L_y/\Delta x = 10, 15, 20, 30, 40, 60$). Fig. 9 shows the map of critical Reynolds numbers of the four LBM schemes, for each pair ($\tau, L_y/\Delta x$). It can be seen that the present scheme is indeed more stable than He and Luo [45] scheme in a wide range of τ and grid resolutions. In this region the critical Reynolds number can be increased around 34% with respect to He and Luo [45] scheme. Also, classical BGK is less stable than the incompressible version (especially for higher τ values) and the Yeomans [46] scheme is much less stable in all tested cases.

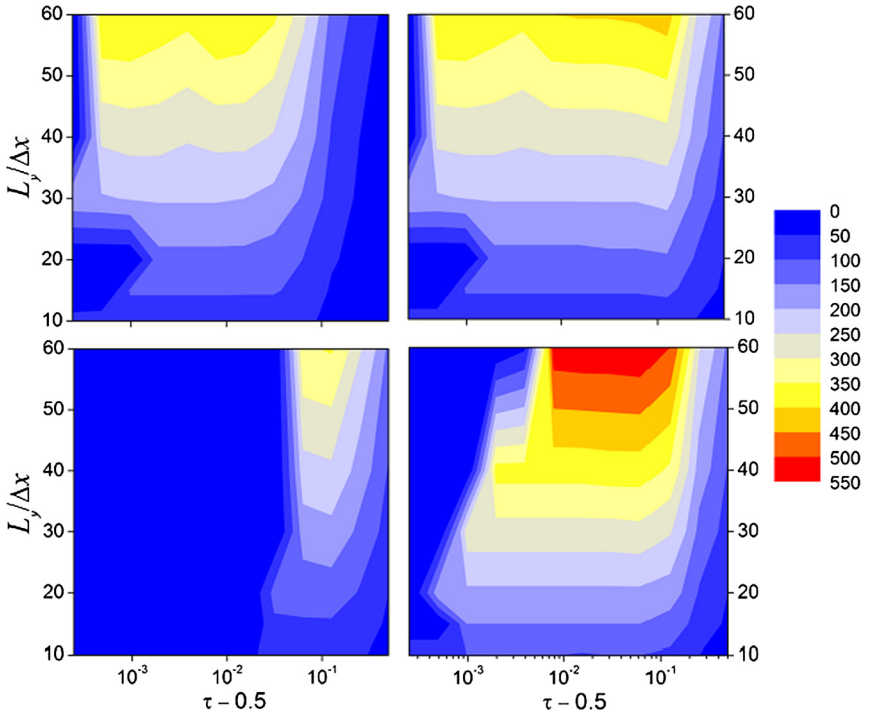

Fig. 9. Map of critical Reynolds number of the Poiseuille flow for the LBM schemes BGK (up-left), He and Luo [45] (up-right), Yeomans [46] (down-left) and present scheme (down-right). (For interpretation of the colors in this figure, the reader is referred to the web version of this article.)

The accuracy of the solutions was assessed by comparison with the analytical solution ($\vec{u}_{exact}$) of the Poiseuille flow. The error is defined then as:

$$error = \frac{\max_j \|\vec{u}(\vec{x}_j, t_n) - \vec{u}_{exact}(\vec{x}_j)\|}{\|\vec{u}_{max}\|}. \tag{35}$$

Fig. 10 displays the map of the errors at the critical Reynolds number (in the same parameter space as Fig. 9), showing that the numerical accuracy of the new method is comparable to He and Luo [45] scheme. In turn, classical BGK and Yeomans [46] schemes are not as accurate.

4.3. Couette flow

The second case consists of numerical simulations of the Couette flow between parallel plates with aspect ratio 2×1, driven by the constant movement of the upper wall. No-slip conditions were applied at the walls (bottom and top), with a constant movement of the top wall (u_{max}) and a fixed pressure at the inlet and the outlet, equal to the initial fluid pressure (p_0).

The initial wall speed is chosen so that the theoretical Reynolds number is 5, that is:

$$u_0 = \frac{\nu\,\mathrm{Re}}{D} = \frac{5\nu}{D}, \tag{36}$$

which is maintained until the criterion for steady state of Eq. (34) is reached. As in the Poiseuille flow, if this criterion is reached in less than $N_T = 80\,(N_P - 1)^2\,/\,(\tau - 0.5)$ time steps, the wall speed (u_{max}) is increased by u_0 and the calculation continues until the steady-state criterion is reached again, and so on. The critical Reynolds is defined as before. The range of the relaxation parameter τ and the number of cells in the transversal direction are also the same as in the previous section.

Fig. 11 shows the map of critical Reynolds numbers of the four LBM schemes for the Couette flow simulation. It can be seen that the present scheme is again more stable than He and Luo [45] scheme for a similar range of τ and grid resolutions. In this region the critical Reynolds number can be increased around 23% respect to He and Luo [45] scheme. While the BGK scheme presents results similar to He and Luo [45] scheme and the Yeomans [46] scheme is again less stable.

The accuracy of the solutions was assessed by comparison with the analytical solution of the planar Couette flow. The error is defined as in Eq. (35). Fig. 12 shows the map of the errors, showing that the numerical accuracy of the proposed scheme is similar to the other schemes in the regions of stability.

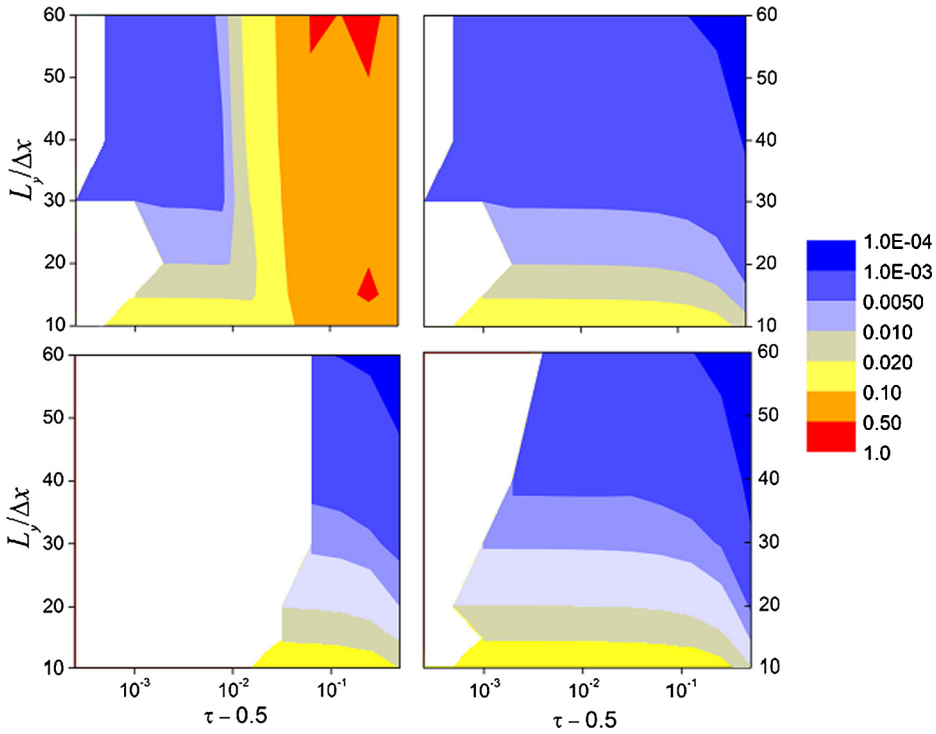

Fig. 10. Map of the error with respect to the analytical solution of the Poiseuille flow for the LBM schemes BGK (up-left), He and Luo [45] (up-right), Yeomans [46] (down-left) and present scheme (down-right). In the white region there is no stable solution. (For interpretation of the colors in this figure, the reader is referred to the web version of this article.)

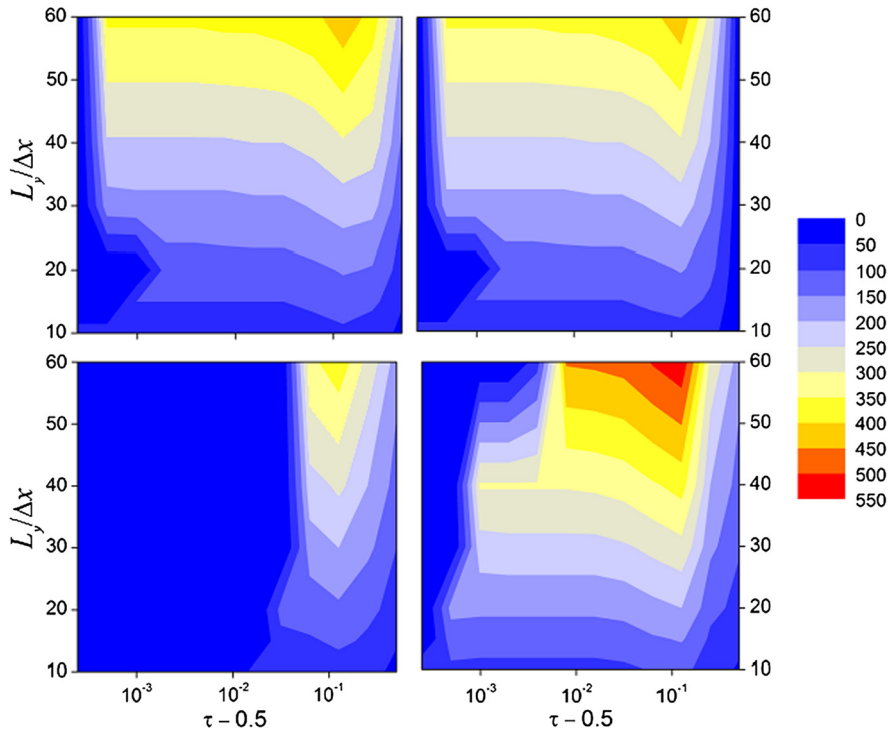

Fig. 11. Map of critical Reynolds number of the Couette flow for the LBM schemes BGK (up-left), He and Luo [45] (up-right), Yeomans [46] (down-left) and present scheme (down-right). (For interpretation of the colors in this figure, the reader is referred to the web version of this article.)

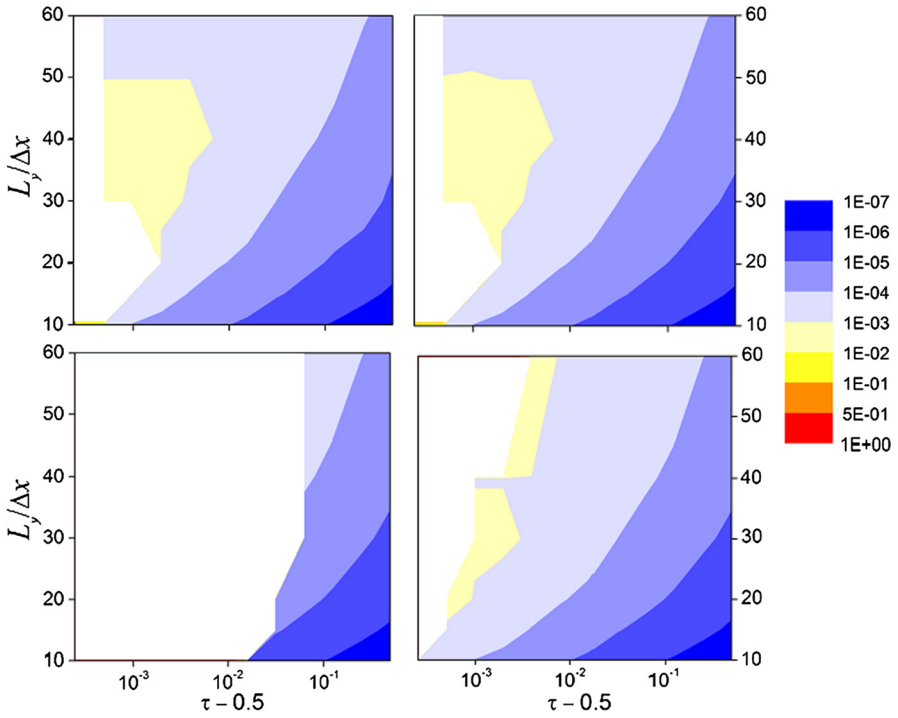

Fig. 12. Map of the error with respect to the analytical solution of the Couette flow for the LBM schemes BGK (up-left), He and Luo [45] (up-right), Yeomans [46] (down-left) and present scheme (down-right). In the white region there is no stable solution. (For interpretation of the colors in this figure, the reader is referred to the web version of this article.)

4.4. Driven Cavity

The last case is the numerical simulation of the Driven Cavity flow, which amounts for simulating the flow of a fluid in a closed rectangular domain with an aspect ratio 2×1 with a no-slip condition at the walls and driven by a constant movement of the top wall (u_{max}).

The initial wall speed is chosen so that the theoretical Reynolds number is 5, that is:

$$u_0 = \frac{\nu \,\mathrm{Re}}{h} = \frac{5\nu}{h}, \tag{37}$$

where h is the height of the cavity. As in the previous cases, if the criterion for steady state of Eq. (34) is reached in less than $N_T = 80(N_P - 1)^2/(\tau - 0.5)$ time steps, the wall speed (u_{max}) is increased by u_0 and the calculation continues until the steady-state criterion is reached again, and so on. The critical Reynolds number, the range of the relaxation parameter τ and the number of cells in the transversal direction is also the same as in the previous sections.

Fig. 13 shows the map of critical Reynolds numbers of each scheme. Note that imposing only velocity boundary conditions leads to achieving stable simulations for much higher Reynolds number (up to 8000) than in the previous cases (up to 550). This is a consequence of the imposition of pressure boundary conditions, even using a method widely adopted in the literature. As this work is focused on the instabilities introduced by the equilibrium distribution, we will not focus on the analysis of methods for imposing boundary conditions. For this special kind of problem, the proposed equilibrium distribution presents improvements in the stability for the least refined meshes. In fact, the compressible and incompressible BGK [45] schemes are slightly more stable in most parts of the map, while the Yeomans [46] scheme is much less stable.

As there is no analytical solution for this problem, the accuracy of the solutions was assessed by comparison with a reference case, chosen as the numerical solution obtained with He and Luo [45] scheme. The error of the other schemes is defined, comparing its velocity field to the reference one ($\vec{u}_{ref}$), at the maximum Reynolds number for which both schemes are considered stable, as:

$$error = \frac{\max_j \|\vec{u}(\vec{x}_j, t_n) - \vec{u}_{ref}(\vec{x}_j)\|}{u_{max}}. \tag{38}$$

Fig. 14 shows the map of the errors in the same parameter space as Fig. 13, showing that the numerical solution of the proposed scheme is close to the one obtained using the He and Luo [45] scheme, in the regions of stability. In turn, classical BGK and Yeomans [46] schemes are not as accurate for the least refined meshes.

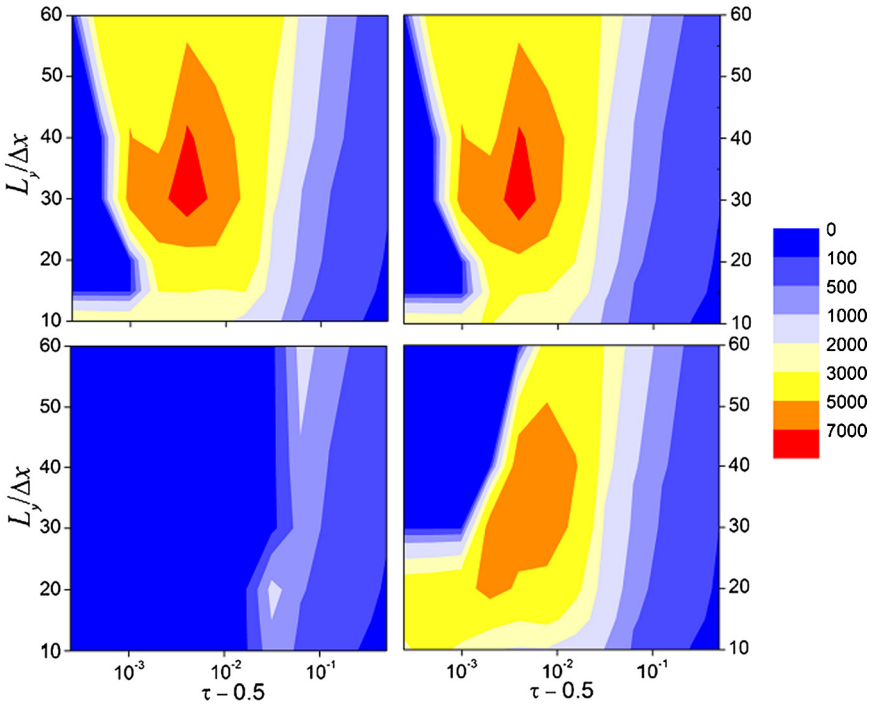

Fig. 13. Map of critical Reynolds number of the Driven Cavity for the LBM schemes BGK (up-left), He and Luo [45] (up-right), Yeomans [46] (down-left) and present scheme (down-right). (For interpretation of the colors in this figure, the reader is referred to the web version of this article.)

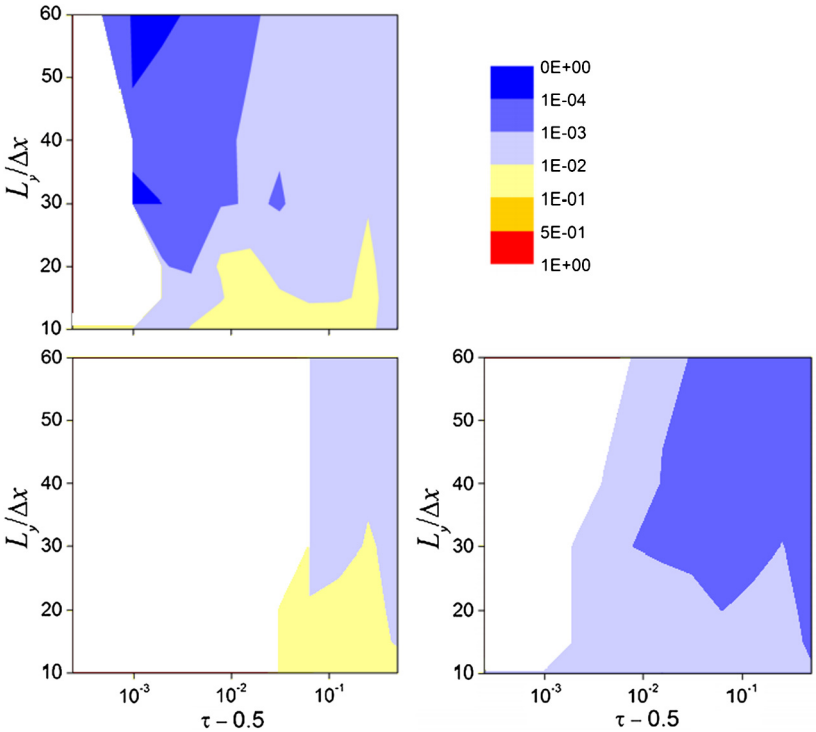

Fig. 14. Map of the difference between the numerical solution, using the LBM scheme He and Luo [45], of the Driven Cavity and other LBM schemes, BGK (up-left), Yeomans [46] (down-left) and present scheme (down-right). In the white region there is no stable solution. (For interpretation of the colors in this figure, the reader is referred to the web version of this article.)

5. Conclusions

The stability of a class of LBM schemes was explored using a heuristic technique guided by the von Neumann linear stability method and an educated selection of the wave-number vectors. The linear stability analysis was simplified by assuming a uniform velocity level over the whole domain, while only the wave numbers of the first harmonic normal to the flow direction were permitted. The relative stability of the members of a two-parameter family of LBM schemes aimed at incompressible flows was studied, identifying a singular equilibrium function that maximizes the critical velocity level. The candidate scheme was afterwards tested in particular cases of confined flows, which are of interest in numerous applications, like pipes and cavities. An important point is that the family of LBM schemes presented is very simple to be implemented and can have great influence in the numerical stability.

In all tested cases the proposed scheme is more stable than other schemes for a certain range of the relaxation parameter and mesh refinement (especially on the least refined meshes). Better results were obtained with this new scheme when pressure boundary conditions were imposed. Particularly, in the Driven Cavity flow (for which the Reynolds numbers are much higher), we clearly noticed that the Reynolds obtained with the least refined meshes was greater in the present scheme, while the other schemes obtain better results as the mesh is refined.

The proposed methodology can be also applied to other classes of LBM schemes, like regularized and higher order distribution functions. Finally, we remark that the results of the present study are concerned with the instabilities introduced by the equilibrium distribution. However, it is also known that the boundary conditions also influence the stability of the scheme. This can be the object of future investigations.

Acknowledgements

This work was supported by the Brazilian agencies CNPq and FAPERJ, specifically by the Program Science without Borders, MEC-MCTI-CAPES-CNPq-FAPs of Brazil.

References

[1] R. Benzi, S. Succi, M. Vergassola, The lattice Boltzmann equation: theory and applications, Phys. Rep. 222 (1992) 145–197, http://dx.doi.org/10.1016/0370-1573(92)90090-M.
[2] Y.H. Qian, D. D'Humières, P. Lallemand, Lattice BGK models for Navier–Stokes equation, Europhys. Lett. 17 (1992) 479, http://dx.doi.org/10.1209/0295-5075/17/6/001.
[3] Y.H. Qian, S. Succi, S.A. Orszag, Recent advances in lattice Boltzmann computing, in: D. Stauffer (Ed.), Annual Reviews of Computational Physics III, World Sci. Pub. Co. Pte. Ltd., Singapore, 1995, pp. 195–242.
[4] M. Hirabayashi, M. Ohta, K. Baráth, D.A. Rüfenacht, B. Chopard, Numerical analysis of the flow pattern in stented aneurysms and its relation to velocity reduction and stent efficiency, Math. Comput. Simul. 72 (2006) 128–133, http://dx.doi.org/10.1016/j.matcom.2006.05.037.
[5] A.M. Artoli, A.G. Hoekstra, P.M.A. Sloot, Optimizing lattice Boltzmann simulations for unsteady flows, Comput. Fluids 35 (2006) 227–240, http://dx.doi.org/10.1016/j.compfluid.2004.12.002.
[6] O. Pelliccioni, M. Cerrolaza, M. Herrera, Lattice Boltzmann dynamic simulation of a mechanical heart valve device, Math. Comput. Simul. 75 (2007) 1–14, http://dx.doi.org/10.1016/j.matcom.2006.08.005.
[7] X. He, G. Duckwiler, D.J. Valentino, Lattice Boltzmann simulation of cerebral artery hemodynamics, Comput. Fluids 38 (2009) 789–796, http://dx.doi.org/10.1016/j.compfluid.2008.07.006.
[8] D.R. Golbert, P.J. Blanco, A. Clausse, R.A. Feijóo, Tuning a lattice-Boltzmann model for applications in computational hemodynamics, Med. Eng. Phys. 34 (2012) 339–349, http://dx.doi.org/10.1016/j.medengphy.2011.07.023.
[9] T. Hyakutake, T. Matsumoto, S. Yanase, Lattice Boltzmann simulation of blood cell behavior at microvascular bifurcations, Math. Comput. Simul. 72 (2007) 134–140, http://dx.doi.org/10.1016/j.matcom.2006.05.010.
[10] M.M. Dupin, I. Halliday, C.M. Care, L.L. Munn, Lattice Boltzmann modeling of blood cell dynamics, Int. J. Comput. Fluid Dyn. 22 (2008) 481–492, http://dx.doi.org/10.1080/10618560802238242.
[11] Y. Liu, A lattice Boltzmann model for blood flows, Appl. Math. Model. 36 (2012) 2890–2899, http://dx.doi.org/10.1016/j.apm.2011.09.076.
[12] D.H. Rothman, S. Zaleski, Lattice-Gas Cellular Automata: Simple Models of Complex Hydrodynamics, Cambridge University Press, Cambridge, 1997.
[13] T. Abe, Derivation of the lattice Boltzmann method by means of the discrete ordinate method for the Boltzmann equation, J. Comput. Phys. 131 (1997) 241–246, http://dx.doi.org/10.1006/jcph.1996.5595.
[14] J.D. Sterling, S. Chen, Stability analysis of lattice Boltzmann methods, J. Comput. Phys. 123 (1996) 196–206, http://dx.doi.org/10.1006/jcph.1996.0016.
[15] R.A. Worthing, J. Mozer, G. Seeley, Stability of lattice Boltzmann methods in hydrodynamic regimes, Phys. Rev. E 56 (1997) 2243–2253, http://dx.doi.org/10.1103/PhysRevE.56.2243.
[16] F. Tosi, S. Ubertini, S. Succi, H. Chen, I.V. Karlin, Numerical stability of Entropic versus positivity-enforcing lattice-Boltzmann schemes, Math. Comput. Simul. 72 (2006) 227–231, http://dx.doi.org/10.1016/j.matcom.2006.05.007.
[17] R.A. Brownlee, A.N. Gorban, J. Levesle, Stability and stabilization of the lattice-Boltzmann method, Phys. Rev. E 75 (2007) 036711, http://dx.doi.org/10.1103/PhysRevE.75.036711.
[18] B. Servan-Camas, F.T.C. Tsai, Non-negativity and stability analyses of lattice-Boltzmann method for advection–diffusion equation, J. Comput. Phys. 228 (2009) 236–256, http://dx.doi.org/10.1016/j.jcp.2008.09.005.
[19] M. Rheinländer, On the stability structure for lattice Boltzmann schemes, Comput. Math. Appl. 59 (2010) 2150–2167, http://dx.doi.org/10.1016/j.camwa.2009.08.040.
[20] D. Ricot, S. Marié, P. Sagaut, C. Bailly, Lattice Boltzmann method with selective viscosity filter, J. Comput. Phys. 228 (2009) 4478–4490, http://dx.doi.org/10.1016/j.jcp.2009.03.030.
[21] M.F. El-Amin, S. Sun, A. Salama, On the stability of the finite difference based lattice Boltzmann method, Proc. Comput. Sci. 18 (2013) 2101–2108, http://dx.doi.org/10.1016/j.procs.2013.05.380.
[22] D.N. Siebert, L.A. Hegele, P.C. Philippi, Lattice Boltzmann equation linear stability analysis: thermal and athermal models, Phys. Rev. E 77 (2008) 026707.
[23] A. Montessori, G. Falcucci, P. Prestininzi, M. La Rocca, S. Succi, Regularized lattice Bhatnagar–Gross–Krook model for two- and three-dimensional cavity flow simulations, Phys. Rev. E 89 (2014) 053317.

[24] L. Zhang, Z. Zeng, H. Xie, Y. Zhang, Y. Lu, A. Yoshikawa, H. Mizuseki, Y. Kawazoe, A comparative study of lattice Boltzmann models for incompressible flow, Comput. Math. Appl. 68 (2014) 1446–1466.
[25] X. Shan, X.F. Yuan, H. Chen, Kinetic theory representation of hydrodynamics: a way beyond the Navier–Stokes equation, J. Fluid Mech. 550 (2006) 413–441, http://dx.doi.org/10.1017/S0022112005008153.
[26] P.C. Philippi, L.A. Hegele Jr, L.O. dos Santos, R. Surmas, From the continuous to the lattice Boltzmann equation: the discretization problem and thermal models, Phys. Rev. E 73 (2006) 056702.
[27] D.N. Siebert, L.A. Hegele Jr, R. Surmas, L.O. dos Santos, P.C. Philippi, Thermal lattice Boltzmann in two dimensions, Int. J. Mod. Phys. C 18 (2007) 546–555.
[28] X. Shan, General solution of lattices for Cartesian lattice Bhatnagar–Gross–Krook models, Phys. Rev. E 81 (2010) 036702.
[29] K.K. Mattila, L.A. Hegele Jr, P.C. Philippi, High-accuracy approximation of high-rank derivatives: isotropic finite differences based on lattice-Boltzmann stencils, Sci. World J. 2014 (2014) 142907.
[30] V. Ansari, A.S. Goharrizi, S. Jafari, B. Abolpour, Numerical study of solid particles motion and deposition in a filter with regular and irregular arrangement of blocks with using lattice Boltzmann method, Comput. Fluids 108 (2015) 170–178.
[31] S. Bogner, S. Mohanty, U. Rüde, Drag correlation for dilute and moderately dense fluid-particle systems using the lattice Boltzmann method, Int. J. Multiph. Flow 68 (2015) 71–79.
[32] A. Fakhari, T. Lee, Numerics of the lattice Boltzmann method on nonuniform grids: standard LBM and finite-difference LBM, Comput. Fluids 107 (2015) 205–213.
[33] S. Gong, P. Cheng, Numerical simulation of pool boiling heat transfer on smooth surfaces with mixed wettability by lattice Boltzmann method, Int. J. Heat Mass Transf. 80 (2015) 206–216.
[34] Y. Hu, D. Li, S. Shu, X. Niu, Study of multiple steady solutions for the 2D natural convection in a concentric horizontal annulus with a constant heat flux wall using immersed boundary-lattice Boltzmann method, Int. J. Heat Mass Transf. 81 (2015) 591–601.
[35] A. Karimipour, A.H. Nezhad, A. D'Orazio, M.H. Esfe, M.R. Safaei, E. Shirani, Simulation of copper–water nanofluid in a microchannel in slip flow regime using the lattice Boltzmann method, Eur. J. Mech. B 49 (2015) 89–99.
[36] M. Sheikholeslamia, M. Gorji-Bandpy, K. Vajravelu, Lattice Boltzmann simulation of magnetohydrodynamic natural convection heat transfer of Al_2O_3–water nanofluid in a horizontal cylindrical enclosure with an inner triangular cylinder, Int. J. Heat Mass Transf. 80 (2015) 16–25.
[37] P.P.A. Swain, G. Karapetsas, O.K. Matar, K.C. Sahu, Numerical simulation of pressure-driven displacement of a viscoplastic material by a Newtonian fluid using the lattice Boltzmann method, Eur. J. Mech. B 49 (2015) 197–207.
[38] Z.-X. Tong, Y.-L. He, A unified coupling scheme between lattice Boltzmann method and finite volume method for unsteady fluid flow and heat transfer, Int. J. Heat Mass Transf. 80 (2015) 812–824.
[39] L.A. Hegele Jr, K.K. Mattila, P.C. Philippi, Rectangular lattice-Boltzmann schemes with BGK-collision operator, J. Sci. Comput. 56 (2013) 230–242.
[40] K.K. Mattila, D.N. Siebert, L.A. Hegele Jr, P.C. Philippi, High-order lattice-Boltzmann equations and stencils for multiphase models, Int. J. Mod. Phys. C 24 (2013) 1340006.
[41] P.C. Philippi, L.A. Hegele Jr, R. Surmas, D.N. Siebert, L.O.E. dos Santos, From the Boltzmann to the lattice-Boltzmann equation: beyond BGK collision models, Int. J. Mod. Phys. C 18 (2007) 556–565.
[42] J. Latt, B. Chopard, Lattice Boltzmann method with regularized pre-collision distribution functions, Math. Comput. Simul. 72 (2006) 165–168.
[43] R. Zhang, X. Shan, H. Chen, Efficient kinetic method for fluid simulation beyond the Navier–Stokes equation, Phys. Rev. E 74 (2006) 046703.
[44] H. Chen, R. Zhang, I. Staroselsky, M. Jhon, Recovery of full rotational invariance in lattice Boltzmann formulations for high Knudsen number flows, Phys. A, Stat. Mech. Appl. 362 (2006) 125–131.
[45] X. He, L.S. Luo, Lattice-Boltzmann model for the incompressible Navier–Stokes equation, J. Stat. Phys. 88 (1997) 927–944, http://dx.doi.org/10.1023/B:JOSS.0000015179.12689.e4.
[46] J.M. Yeomans, Mesoscale simulations: lattice Boltzmann and particle algorithms, Physica A 369 (2006) 159–184, http://dx.doi.org/10.1016/j.physa.2006.04.011.
[47] Z. Guo, C. Zheng, B. Shi, An extrapolation method for boundary conditions in lattice Boltzmann method, Phys. Fluids 14 (2002) 2007–2010, http://dx.doi.org/10.1063/1.1471914.
[48] Q. Zou, X. He, On pressure and velocity boundary conditions for the lattice Boltzmann BGK model, Phys. Fluids 9 (2002) 1591–1598, http://dx.doi.org/10.1063/1.869307.